Journal of Controlled Release 128 (2008) 241–247

Contents lists available at ScienceDirect

Journal of Controlled Release

journal homepage: www.elsevier.com/locate/jconrel

NANOTECHNOLOGY

Modular drug transporters with diphtheria toxin translocation domain form edged holes in lipid membranes

Yuri V. Khramtsov [a], Tatyana I. Rokitskaya [b], Andrey A. Rosenkranz [a,c], Georgiy A. Trusov [c], Nikolay V. Gnuchev [a], Yuri N. Antonenko [b], Alexander S. Sobolev [a,c,*]

[a] Department of Molecular Genetics of Intracellular Transport, Institute of Gene Biology, Russian Academy of Sciences, 34/5 Vavilov St., Moscow, 119334, Russia
[b] A.N. Belozersky Institute of Physico-Chemical Biology, Moscow State University, Vorobyevy Gory, Moscow, 119992, Russia
[c] Department of Biophysics, Biological Faculty, Moscow State University, Vorobyevy Gory, Moscow, 119992, Russia

ARTICLE INFO

Article history:
Received 17 December 2007
Accepted 6 March 2008
Available online 19 March 2008

Keywords:
Diphtheria toxin translocation domain
Modular recombinant drug transporters
Membrane pores
Ion channels
AFM

ABSTRACT

Modular/chimeric recombinant drugs or drug transporters usually contain a special translocation domain from bacterial toxins, e.g. diphtheria toxin, as a module enabling escape of the chimeric molecules from acidifying endosomes. This approach is limited by the shortage in the knowledge about the precise molecular mechanisms of translocation of diphtheria toxin and the toxin-based chimera across the endosomal membrane and its release into the cytosol. We present experimental data with the modular recombinant drug transporters (MRTs), containing the translocation domain of diphtheria toxin, developed by us earlier, demonstrating that the MRTs interact with lipid membranes (liposomes, free-standing and supported bilayer lipid membranes) and produce defects in them at endosomal pH's which are sufficient for escape of macromolecules: — MRTs induced leakage of calcein-loaded liposomes pH 3–6.5. Large fluctuating conductance states of 2–5 nS are formed in membranes at pH 5.5. Atomic force microscopy revealed two different types of defects in the supported lipid bilayers at pH 5.5: 1) giant pores (50–200 nm diameters) and 2) small depressions/holes (30–50 nm) produced by the MRTs which are inserted into the membranes thus forming the structures described above. The last was shown with the use of cantilever tips modified with anti-MRT antibodies.

1. Introduction

In the past decade there was a burst of development and trials of novel fusion recombinant drugs, usually anti-tumor drugs, or modular transporters for these drugs. Most of them exploit a process of receptor-mediated endocytosis that occurs both in normal and target cancer cells. Using this process permits to achieve at least two goals: 1) cell-specificity resulted from binding of a fusion drug or transporter to a specific internalizable receptor over-expressed on the target cells and 2) internalization of the drug/transporter by the target cells as a natural step following the binding to the internalizable receptors. Upon internalization, the drug/transporter turns out to be within a closed membraneous vesicle which in most cases separates it from the place of its destination. This problem is usually solved by inclusion of a special component – a part of a bacterial toxin, diphtheria or *Pseudomonas*, which accomplishes escape of the toxins from such vesicles – into the fusion drugs/transporters. The final chimeric proteins containing either translocation domain, T, or its combination with a catalytic one, C, from diphtheria toxin (DT) were obtained and demonstrated their ability to escape from endocytotic vesicles: e.g., a) a protein consisting of catalytic and translocation domains of DT fused to interleukin-3 [1], b) a similar truncated DT fused to two repeating sFv subunits recognizing CD19 and CD22 receptors of B-cell leukemia/lymphoma [2], c) a similar truncated DT fused to ligands enabling targeting human interleukin-13 receptor and urokinase-type plasminogen activator receptor [3], d) a chimeric protein consisting of receptor and translocation domains of DT fused with proapoptotic Bad protein [4]. We [5,6] have designed and produced e) a series of modular recombinant transporters targeting the nuclei of different cancer cells and consisting of: (*i*) an internalizable ligand module providing for target cell recognition and subsequent receptor-mediated endocytosis; (*ii*) an endosomolytic module ensuring escape of the transporter from endosomes, a T-domain of DT; (*iii*) a module containing a nuclear localization sequence (a sequence of amino acids that is recognized by importins needed for the active translocation into the nucleus); and (*iv*) a carrier module for attachment of an anti-tumor agent. Anti-tumor drugs (e.g., photosensitizers, alpha-emitters) acquired cell-specificity and significantly higher efficacy (10–1000 times) when they have been delivered by the transporters to the target cells and into their nuclei which are the most vulnerable to photosensitizers and alpha-particles. Some of chimeric proteins with the truncated DT were

* Corresponding author. Department of Molecular Genetics of Intracellular Transport, Institute of Gene Biology, Russian Academy of Sciences, 34/5 Vavilov St., 119334, Moscow, Russia. Tel.: +7 499 135 3100; fax: +7 499 135 4105.
E-mail address: sobolev@igb.ac.ru (A.S. Sobolev).

0168-3659/$ – see front matter © 2008 Elsevier B.V. All rights reserved.
doi:10.1016/j.jconrel.2008.03.011

tested clinically: these were fusion proteins comprising T- and C-domains of DT fused either with a) interleukin-2 in order to treat cutaneous T-cell lymphoma, chronic lymphocytic leukemia, non-Hodgkin's lymphoma [7–9], or granulocyte–macrophage colony stimulating factor for treatment of acute myelogenous leukemia [10], or epidermal growth factor for carcinoma treatment [11]. The first chimeric protein containing interleukin-2 has been recently approved by the US Food and Drug Administration for the treatment of advanced cutaneous T-cell lymphoma [12].

Although much is known about the mechanisms of receptor-binding and receptor-mediated endocytosis of native DT (58 kDa), little is known about the precise molecular mechanisms of C-domain translocation across the endosomal membrane and its release into the cytosol. Unfolding of the C-domain was postulated more than 25 years ago as a prerequisite for translocation of the domain [13,14]. Later, the idea about the necessity for complete denaturation of the C-domain before translocation was experimentally supported by Olsnes' group [15,16]. At present, there are two competing hypotheses differently explaining translocation of the DT C-domain across the early endosomal membrane: 1) T-domain itself exhibits chaperonin-like properties and is solely sufficient to promote C-domain delivery across the bilayer [17,18], and 2) C-domain translocation across the vesicle membrane is dependent on ATP and the presence of cytosolic components including chaperonin heat shock protein 90 [19]. Nevertheless, the unfolding/denaturation step of the transported domain either by T-domain or by an intracellular chaperonin is explicitly included into the both hypotheses. After C-domain translocation, it is enzymatically cleaved from the whole DT at a special cleavage site, which is located near the N-terminus of T-domain, and is released into the cytosol [20]. Concerning fusion proteins containing the DT T- and C-domains and, especially, the modular recombinant transporters with molecular weights ≥70 kDa, it seems not obvious that other different components of the transporters or fusion proteins — e.g., interleukins-2, -3, -13, granulocyte–macrophage colony stimulating factor, epidermal growth factor, sFv subunits and others like *E. coli* hemoglobin-like protein HMP (43.9 kDa) that were included into the chimeras as carrier modules/domains — can be easily and reversibly unfolded in order to escape from endosomes. Moreover, the modular recombinant transporters possessed T-domains (202–384 a.a. residues of the whole DT) lacking the cleavage site, and this T-domain located either between other modules or, usually, directly at N-terminus of the whole transporter. However, the transporters do escape from endocytotic compartments and reach places of their subcellular destination [5,6]. The increasing number of newly produced artificial chimeric proteins comprising the DT T-domain for endosomal escape and absence of explanation of their membrane activity stimulated us to undertake some steps towards elucidation of the mechanisms of this activity. Moreover, we believe that experiments with artificial chimeras containing the DT T-domain may help to shed some light on the still obscure process of the DT translocation. Here, we present our experimental data with the modular recombinant transporters (MRTs), containing the DT T-domain, developed by us earlier demonstrating that the MRTs interact with artificial membranes (liposomes, supported lipid bilayers, planar bilayer lipid membranes) and produce defects in them at slightly acidic pH's which are sufficient for escape of macromolecules. These defects are produced by MRTs which inserted into the membranes forming different structures.

2. Materials and methods

2.1. Modular recombinant transporters (MRTs)

The MRTs, T–HMP–NLS–αMSH (70.4 kDa), T–HMP–NLS–EGF (76.3 kDa), HMP–NLS–αMSH (50.1 kDa), T–αMSH (20.8 kDa) and HMP (43.9 kDa) where: T, translocation domain of DT, an endosomolytic module; HMP, *E. coli* hemoglobin-like protein, a carrier module; NLS, optimized SV40 large T–antigen nuclear localization sequence, αMSH, alpha-melanocyte stimulating hormone, and EGF, human epidermal growth factor, ligand modules, were produced and purified as described previously [5,6].

2.2. Interaction of the MRTs with small unilamellar liposomes at different pH's

Egg lecithin (KhimFarmZavod, Kharkov, Ukraine) was used without further purification. Small unilamellar liposomes were prepared according to Szoka and Papahadjopoulos [21] by sonicating fresh lipid suspension in 20 mM HEPES, 20 mM MES, 20 mM citrate, 150 mM NaCl, pH 7.5 buffer until clear, using a W-181-T sonicator (Finnsonik, Lahti, Finland; 40 kHz, 90 W, 0 °C, 30 min), and passed several times through 0.45 and 0.22 μm filters (Corning, Corning, NY). A part of the liposomes were used in order to obtain supported bilayers (see below). Another part of the liposomes were loaded with fluorescent calcein (3,3′-bis[*N*,*N*-bis(carboxymethyl)aminomethyl]fluorescein; 623 Da) up to the concentration of fluorescence quenching and its leakage under the MRT action at pH 3–7.5 was tested according to Rosenkranz et al. [22].

2.3. Interaction of the MRTs with supported bilayers at different pH's

A Digital Instruments Multimode Scanning Probe Microscope on a Nanoscope IIIa (Veeco Instruments, Woodbury, NY) controller fitted with J-scanner (165 μm maximum scan size) and a Tapping Mode Liquid Cell were used to image the lipid bilayer *in situ*. A piece of mica was attached to the 1.6-cm diameter metal disk supplied by Veeco and was installed in the microscope. The Tapping Mode Liquid Cell was fitted with inlet and outlet tubing to allow exchange of solutions in the cell during imaging. Samples of supported unilamellar bilayers were prepared by the vesicle-fusion method as described by Puntheeranurak et al. [23]. There were used liposomes made of egg lecithine described above as well as the liposomes made of diphytanoyl phosphatidyl glycerol (DPhPG) and diphytanoyl phosphatidyl choline (DPhPC) (3:7, w/w; both from Avanti Polar Lipids, Alabaster, AL) in 20 mM MES-Tris, 150 mM NaCl pH 7.5 according to Sobko et al. [24] and stored in dark under nitrogen at 4 °C. Briefly, a drop either of about 100 μl of the lecithin suspension (3–5 μg/ml) or of about 80 μl of the DPhPG–DPhPC suspension (23 μg/ml with 2 mM Mg^{2+}) was applied to a piece of freshly cleaved mica, allowing incubation at room temperature for 15 min, then the Tapping Mode Liquid Cell was sealed using a Teflon O-ring and flushed with fresh buffer (20 mM HEPES, 20 mM MES and 150 mM NaCl, pH 7.5) to remove any excess lipid before imaging. Specimens were imaged to check for bilayer. Oxide-sharpened silicon nitride V-shaped cantilevers with a nominal force constant of 0.06 N/m were used and the forces were minimized during the scans. For force measurements studies real spring constants of cantilevers (0.063–0.083 N/m) were determined as described [25]. Briefly, a silicon cantilever (Digital Instruments, Santa Barbara, CA) with a spring constant of k_{ref} = 0.164 ± 0.007 N/m was taken as reference cantilever. The silicon nitride cantilevers were calibrated by comparing their repulsive force–distance slopes on a solid support with slopes found in contact with the reference cantilever. Spring constants k_{test} were determined using the relation $k_{test} = k_{ref}(\delta_{tot}/\delta_{test} - 1)/\cos\theta$, where δ_{tot} and δ_{test} are the slopes measured on a solid support and on the reference cantilever, respectively, and θ is the angle between the cantilever under test and the reference cantilever. All silicon nitride cantilevers were calibrated with the same reference cantilever. The silicon nitride cantilevers were irradiated with UV light prior to imaging to remove any adventitious organic contaminants. All measurements were performed in contact and tapping modes (cantilever drive frequencies ~9 kHz) at room temperature using tip scan rate about 2–4 Hz. All images were captured as 256 × 256 or 512 × 512 pixel images and were flattened and smoothed.

2.4. Identification of MRTs in the supported lipid bilayers with the use of antibodies coupled to a cantilever tip

Anti-MRT polyclonal antibodies were raised in rabbits and affinity purified [6]. Tip modification was carried out according to the Cai and Yang method [26,27]. Briefly, NP-S cantilever was incubated in 35% HCl/methanol (1:1 v/v) for 30 min, washed with methanol and incubated in 0.5% methanol-diluted 3-(trimetyloxysilyl)propyl metacrylate (Fluka, Seelze, Germany) for 45 min and washed with methanol and water. Finally, the cantilever was incubated in 0.2% (weight) ammonium peroxodisulfate, 0.2% (volume) *N,N,N′,N′*-tetramethylethylenediamine (both from Fluka) and 5 μg/ml anti-MRT antibodies for 45 min and washed with water and 50 mM phosphate buffer at pH 8.

2.5. Electrophysiological characterization of interaction of the MRTs with planar bilayer lipid membranes (BLM) at different pH's

BLM were formed from a 2% solution of lipid in decane by the brush technique [28] on a 0.5-mm diameter hole in a Teflon partition separating two compartments of a cell containing aqueous solutions of 20 mM MES, 20 mM Tris и 150 mM KCl, pH 5.5 or 7.5. Lipid mixture contained DPhPG and DPhPC (30:70% by moles). MRT were added from stock solution to *cis* side of the membrane with permanent stirring. The recording was carried out without stirring to reduce the electrical noise. The electrical current (I) was measured with a patch-clamp amplifier (model BC-525C, Warner Instruments, Hamden, CT), digitized by a LabPC 1200 (National Instruments, Austin, TX), and analyzed by a personal computer with the help of WinWCP Strathclyde Electrophysiology Software designed by J. Dempster (University of Strathclyde, UK). The current was low-pass filtered with a cutoff frequency of 100 Hz. Ag–AgCl electrodes were placed directly into the cell.

3. Results

3.1. MRTs make defects in liposomes loaded with calcein permitting calcein efflux from the liposomes

The propensity of a polypeptide to make pores in membranes in an acidic medium can be assessed from its ability to induce leakage of dye-loaded liposomes at different pH's [29]. Fig. 1A shows the pH dependence of calcein leakage induced by T–HMP–NLS–αMSH, by truncated MRT HMP–NLS–αMSH lacking T-domain, by HMP, and by the T-domain fused with αMSH. All the proteins induced calcein leakage at acidic pH (from pH 3.5 to pH 4.5) while only T–HMP–NLS–αMSH and T–αMSH were active at pH from 4.5 to 6.5, i.e. the region close to the endosomal pH [30]. It can be concluded that the activity at these slightly acidic pH region can be attributed to the activity of the endosomolytic module of the complete MRT, the DT T-domain.

Similar results were obtained with EGF-containing MRTs [6]. Concentration dependence of liposome leakage induced by T–HMP–NLS–αMSH, HMP–NLS–αMSH, and T–αMSH (Fig. 1B) suggests synergistic influence of HMP module on membranolytic action of the T module resulting in a leakage at significantly lower concentrations of a complete MRT, T–HMP–NLS–αMSH, if compared with T–αMSH or truncated MRT, HMP–NLS–αMSH.

3.2. MRTs induced ion channels in planar bilayer lipid membranes

Bilayer lipid membranes were used to study the induction of electrical current by T–containing T–HMP–NLS–αMSH and its T-free analogue, HMP–NLS–αMSH, at pH 5.5 and 7.5. It was found that the 10–20 min incubation of T–HMP–NLS–αMSH with BLM at pH 5.5 led to the induction of stepwise increase in the ionic current, the amplitude of which were in the range of 2–5 nS. Fig. 2A represents a typical record of the T–HMP–NLS–αMSH-mediated opening of two channels with conductances of 2.8 and 4.2 nS. Changes in ion current have not been recorded in the absence of MRTs either at pH 5.5 or at pH 7.5 (data not shown). The characteristic features of these channels were large variation of step conductances and also instability in the level of the channel conductance. Fig. 2A, inset, shows the increased width of the histogram of the second and the third current levels compared to the first which is determined by the noise of the amplifier. Interestingly, the closing events were not observed (4 independent experiments, total time of observation was 50 min), suggesting that these opening states were very stable. Substantially different behavior of T–HMP–NLS–αMSH-mediated current was observed at pH 7.5. The interaction of the T–HMP–NLS–αMSH with the membrane led to fast flickering of the current with irregular amplitudes without formation of stable channels (5 independent experiments, total time of observation was 130 min). Typical record of the current is shown in Fig. 2B. It is hard to estimate the amplitude and duration of the current openings due to their variation in amplitudes and the shortness (see inset).

We studied the action of HMP–NLS–αMSH lacking T-domain under the same conditions. This protein induced fluctuations of the membrane current upon the addition at pH 5.5 which occasionally disappeared (Fig. 3A). However, in part of our experiments (30%) large openings of stable channels were observed as shown on the inset to Fig. 3A (conductance 3.3 nS). In a majority of recordings (5 independent experiments) these stable channel openings did not appear. HMP–NLS–αMSH did not induce stable channels at pH 7.5 (4 independent experiments, total time of observation was 55 min) although it induced the flickering of the current (Fig. 3B).

3.3. MRTs produce defects in the supported lipid bilayers as revealed by atomic force microscopy

Membrane defects produced by T–HMP–NLS–EGF were assessed with the use of atomic force microscopy (AFM) on supported egg

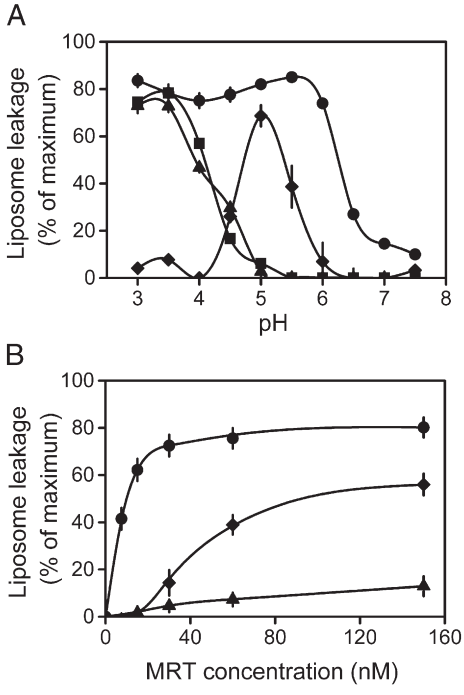

Fig. 1. Liposome leakage induced by MRTs. A, pH dependence. T–HMP–NLS–αMSH (●), HMP–NLS–αMSH (▲), T-αMSH (♦) and HMP (■). Egg yolk phosphatidylcholine liposomes were loaded with fluorescent calcein up to the concentration of fluorescence quenching; the liposome leakage resulted in appearance of fluorescence. B, Concentration dependence. T–HMP–NLS–αMSH (●), HMP–NLS–αMSH (▲), and T-αMSH (♦) were added at indicated concentrations to calcein-loaded liposomes at pH 5.5. After incubation of liposomes with the indicated MRTs, pH of every specimen had been adjusted to the same value, pH = 7.5, before fluorescence measurements.

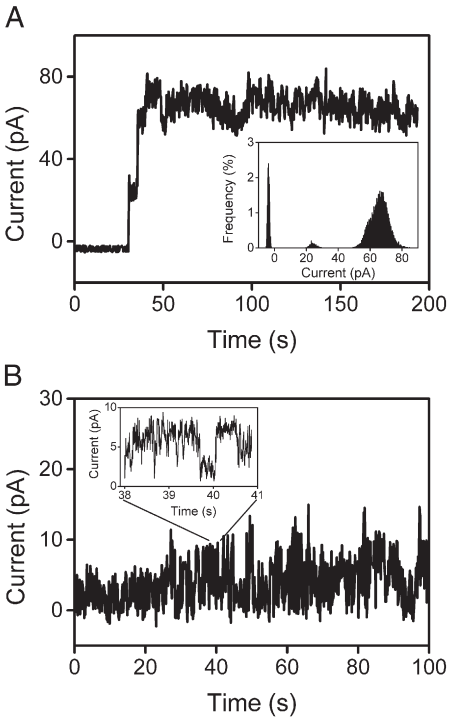

Fig. 2. Single channel trace of T–HMP–NLS–αMSH (16 nM) in planar lipid bilayer membrane at 10 mV. A, pH 5.5. Inset: corresponding current amplitude histogram. B, pH 7.5. Inset: expanded part of the record.

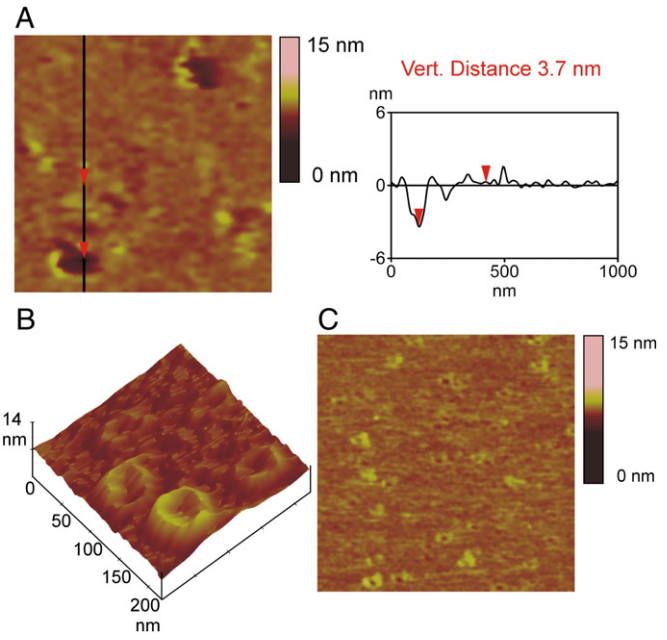

Fig. 4. Action of 5 nM MRT on lipid bilayer of egg phosphatidyl choline at pH 5.5. A, T–HMP–NLS–EGF, atomic force microscopy contact mode height image (1×1 μm; *z*-scale, 14 nm; scan rate 3 Hz). The cross section taken along the black line is shown on the right part of the figure; the distance between the red triangles is 3.7 nm. B, T–HMP–NLS–EGF, higher magnification than on A. Atomic force microscopy tapping mode height image (222×222 nm; *z*-scale, 14 nm; scan rate, 2 Hz). C, HMP–NLS–αMSH, atomic force microscopy tapping mode height image (1×1 μm; *z*-scale, 15 nm; scan rate, 3 Hz).

lecithin bilayers (Fig. 4A). After addition to the bilayer (at pH 7.5) and pH adjustment to 5.5, the MRT caused formation of two types of defects in previously intact parts of the bilayer: (*i*) fluctuating holes, partially edged with "heights" (Fig. 4A), with typical diameters ranging from 50 nm to 200 nm which depth, 35–50 Å, corresponds to the bilayer thickness, and (*ii*) small depressions or holes with diameters of 30–50 nm (Fig. 4B) surrounded by circular "ramparts". The MRT did not cause the fluctuating holes at pH 7.5 (data not shown).

Interestingly, the circular structures with "ramparts" have been revealed after addition of the MRT lacking DT T-domain, HMP–NLS–αMSH, to egg lecithin bilayers and pH adjustment to 5.5 (Fig. 4C). This suggests that formation of circular "ramparts" is not due to DT T-

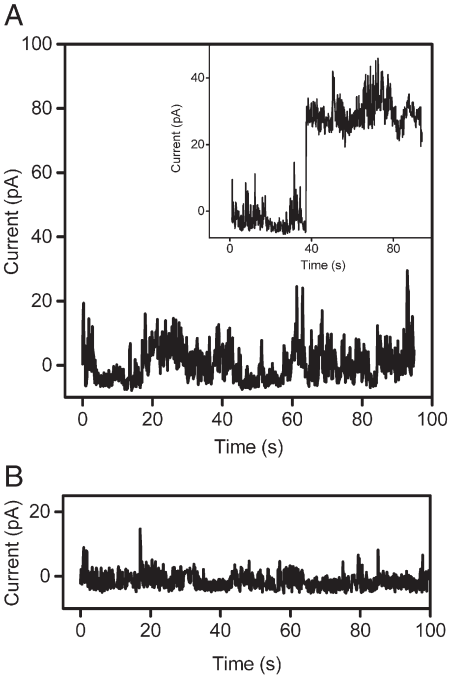

Fig. 3. Single channel trace of HMP–NLS–αMSH (24 nM) in planar lipid bilayer membrane at 10 mV and pH 5.5 (A) and pH 7.5 (B). Inset: an example of the opening of large conductance state.

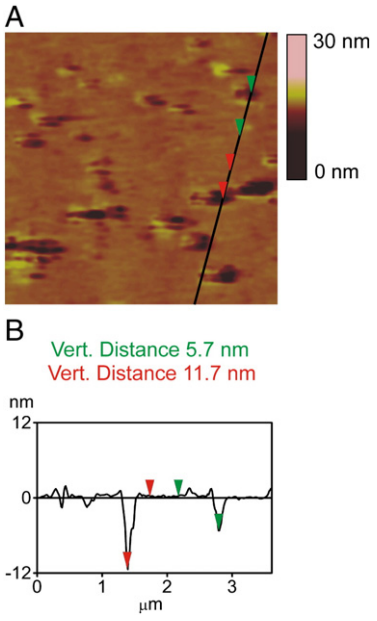

Fig. 5. 30 nM T–HMP–NLS–EGF added to the bilayers of DPhPG–DPhPC (30:70) at pH 5.5. A, atomic force microscopy contact mode height image (3.5×3.5 μm; *z*-scale, 30 nm; scan rate 4 Hz). B, the cross section taken along the black line; the distance between the green triangles is 5.7 nm and the distance between the red triangles is 11.7 nm.

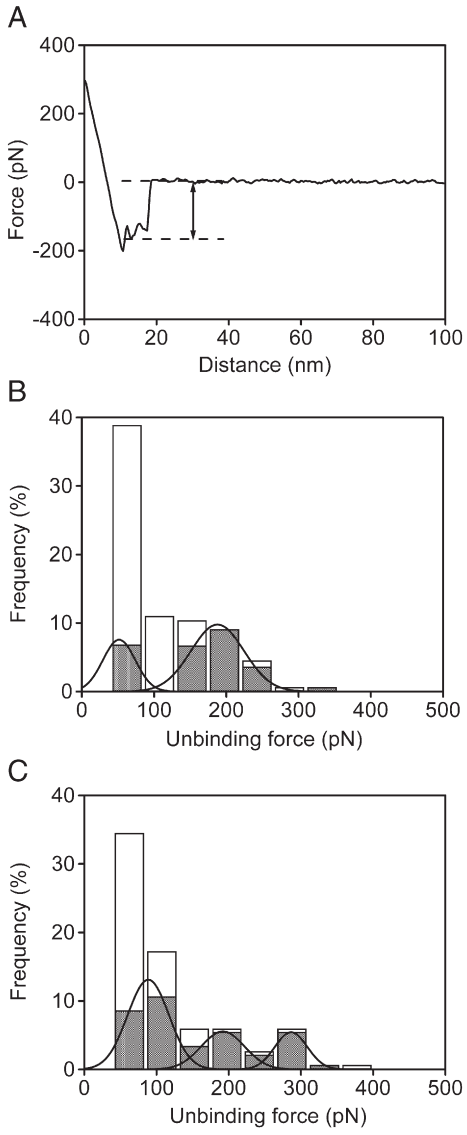

Fig. 6. Frequency distribution of forces of interaction between anti-MRT antibodies and the structures revealed after 30 nM T–HMP–NLS–EGF MRT incubation with the supported egg lecithin bilayers (pH 5.5). A, a typical curve for a modified with anti-MRT antibodies tip interacting with T–HMP–NLS–EGF MRT on the supported bilayer. The length of the arrow corresponds to the interaction force between the modified tip and the sample. The 1st peak resulted from non-specific interaction of the tip with the supported lipid bilayer or mica and was not taken into account. Frequency distributions have been recorded at rates 100 nm/s (B) and 400 nm/s (C) of retraction of the modified tip. Differences (grey bars) between the corresponding experiment (tips modified with specific anti-MRT antibodies; total bars) and control (tips modified with unspecific anti-β-galactosidase antibodies; open bars) have been used for calculations of separate Gauss curves. Only forces higher than 40 pN (noise level) had been taken into account. The calculations were made assuming that unbinding forces within one group did not vary more than by 45 pN. Peak maxima: B, 100 nm/s: 52 pN and 188 pN; C, 400 nm/s: 88.7, 192, and 286 pN.

domain action but rather due to another membrane active module of the MRT: *E. coli* hemoglobin-like protein HMP.

The holes, similar to those shown in Fig. 4A, have been revealed after addition of T–HMP–NLS–αMSH to DPhPG–DPhPC bilayer at pH 5.5 (Fig. 5A); the defects have not been detected at pH 7.5 (data not shown). These holes began to appear at higher concentrations of T–HMP–NLS–αMSH (>25 nM) than in egg phosphatidyl choline bilayer (≥5 nM), possibly as a result of negative charge of the DPhPG–DPhPC bilayer. Interestingly, T–HMP–NLS–αMSH is able to make holes in double bilayers which DPhPG–DPhPC can form sometimes on mica (Fig. 5B, red triangles, compare with green triangles).

3.4. Defects, produced by MRTs in the supported lipid bilayers, are surrounded with MRTs as revealed by biospecific AFM

Several force curves for different tip − sample interactions have been recorded: unmodified/modified tip – supported bilayer-on-mica, and unmodified/modified tip – MRTs on the supported bilayer as well as for a tip modified with non-specific anti-β-galactosidase antibodies. A typical force curve for interaction of a tip, modified with anti-MRT antibodies, with T–HMP–NLS–EGF MRT on the supported bilayer is shown in the Fig. 6A. The 1st peak is usually observed even during tip/bilayer-on-mica interactions (data not shown) and is probably resulted from unspecific interactions between the tip and lipid bilayer/mica; this peak had not been taken into account at further calculations.

The part of the curve which is parallel to *X*-axis corresponds to a free, non-interacting tip. It was possible to observe 1–4 peaks – apart from the above-mentioned 1st peak – that may be explained as interaction of several antibodies coupled to the tip with different antigens of the sample [26,31].

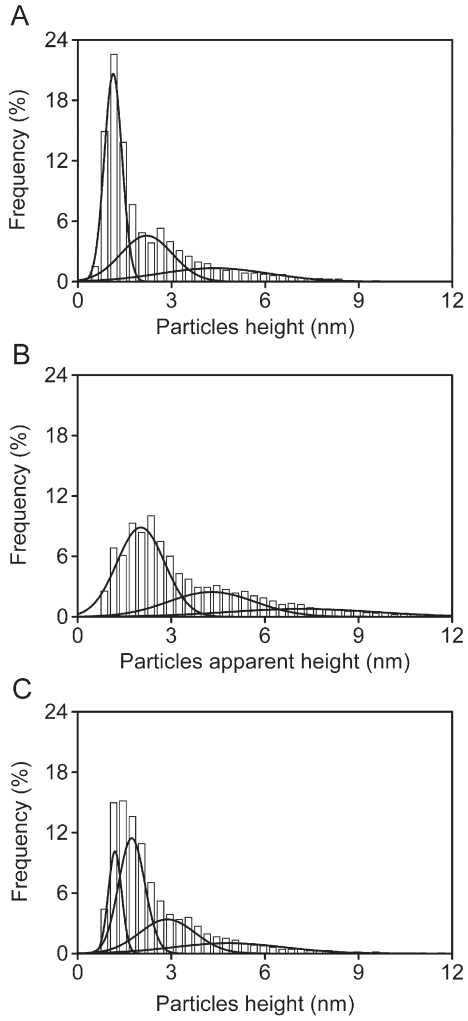

Fig. 7. Frequency distribution of particle heights on/in the surface of the supported egg lecithin bilayer incubated with T–HMP–NLS–EGF at pH 5.5 with the use of unmodified tip (without addition of antibodies to the bilayer) (A), with anti-MRT antibody-modified tip (without addition of antibodies to the bilayer) (B), and with unmodified tip after addition of antibodies to the bilayer (C). The calculations were made assuming that particles within one group did not vary in size more than by 3 Å. Only particles higher than 4 Å (cantilever noise level) had been taken into account. Peak maxima: A, 1.1 ± 0.1 nm, 2.2 ± 0.2 nm, and 4.4 ± 1.9 nm (correlation coefficient $r = 0.995$); B, 2.0 ± 0.1 nm, 4.3 ± 0.6 nm, and 7 ± 2 nm ($r = 0.985$); C, 1.2 ± 0.1 nm, 1.7 ± 0.1 nm, 2.9 ± 0.3 nm, and 4.8 ± 1.6 nm ($r = 0.999$).

Because the interaction force depends on the retraction rate of a modified tip, the measurements had been carried out at 2 different tip retraction rates: 100 and 400 nm/s. The frequency distribution of the forces of specific interactions are shown in the Fig. 6B and C. Because we used polyclonal antibodies, so the first two peaks in the Fig. 6B and C may be attributed to two types – weak and strong – antibody–antigen interaction. Thus, an average force for one strong antibody–antigen (MRT) interaction can be estimated as approx. 192 pN, this value corresponds to the published data [32,33]. The average value of the 3rd peak, 286 pN, which appeared at higher rates of tip retraction, is more than the that of the 2nd peak, 192 pN, and suggests a break of two antibody–antigen interactions [32]. The obtained results allow to conclude that the tip successfully modified with the antibodies recognized MRTs in the supported lipid bilayers.

Additional evidence for the presence of MRTs on/in the egg lecithin bilayer were obtained from scanning the bilayer incubated with T–HMP–NLS–EGF at pH 5.5 with tips either modified with anti-MRT antibodies or unmodified; totally ~12,000 particles were scanned and counted with the use of "Particle analysis" program (Veeco). Scanning with an unmodified tip revealed three types of particles with mean heights of 1.1, 2.2 and 4.4 nm (Fig. 7A), whereas scanning of the specimens with anti-MRT antibody-modified tip gave three types of particles, too, but the first two types turned out to be significantly ($p<0.001$) higher: 2.0, 4.3 and 7 nm (Fig. 7B). The apparent "enlargement" is typical to antigen–antibody interaction revealed by AFM [34]. Mean height of antibodies on mica was measured by AFM and was 0.7±0.5 nm (data not shown). It is known that addition of antibodies to a surface containing corresponding antigens on it makes these antigens "higher" by approx. 1 nm [35,36]. Addition of anti-MRT antibodies to the bilayers with T–HMP–NLS–EGF at pH 5.5 caused the similar effect (Fig. 7C). The 1st peak became divided into two peaks (Fig. 7C). The new 1st peak with height (1.1–1.2 nm), equal to that before antibody addition, seems to correspond to particles which do not interact with the antibodies, whereas the 2nd is significantly ($p<0.001$) higher by 0.6 nm.

All the above data suggest that all the particles detected on/in the supported bilayer are MRT molecules which can be either inserted in it (Fig. 7A, peak of low particles) or adsorbed (Fig. 7A, peak of mid-height particles) or aggregated on its surface (Fig. 7A, peak of high particles).

4. Discussion

Formation of defects in model lipid membranes by MRTs containing the DT T-domain as an endosomolytic module has been demonstrated with the use of three independent approaches: 1) a leakage of calcein-loaded liposomes, 2) formation of ion channels in planar bilayer lipid membranes, and 3) different variants of AFM.

The pH dependence of MRT-induced leakage of calcein-loaded liposomes suggested two modes of action of the MRTs: the first one which can be revealed at pH 4.5–6.5 and is attributable to the activity of the DT T-domain, and the second activity characteristic of pH 3.5–4.5 and attributable to the HMP. The membrane activity of HMP was firstly demonstrated by us [5] and subsequently and independently shown by the group of A. Boffi for *E. coli* and *Vitreoscilla stercoraria* HMPs [37,38]. Interestingly, HMP module synergistically affects the membranolytic action of T module resulting in formation of membrane defects at significantly lower MRT concentrations.

Electrophysiological characterization of membrane defects which probably resulted in calcein leakage are shown in Figs. 2 and 3. The data suggested the formation of large conductance states in the range of 2–5 nS at pH 5.5. This conductance level corresponded to pores of the diameter of about several nanometers [39] which ensure the permeation of calcein and larger molecules. The conductance states can be hardly attributed to ion channels with defined geometry because of the fluctuations in the open current level. Rather, it may be assumed that T–HMP–NLS–αMSH forms channels with flexible geometry leading to instability in the open state conductance. Basing upon ASM data, one may assume that these channels can interact and form big fluctuating holes presumably via fusion with each other. The change in the pH to 7.5 led to change in protein interaction with the membrane. Namely, the protein induced flickering of the current without induction of large channels.

Truncated MRT, HMP–NLS–αMSH, lacking T-domain, had reduced ability to form ion channels at pH 5.5 (channel openings were observed only in 30% of experiments) compared to T-HMP–NLS–αMSH which induced large pores in all the experiments conducted. It can be assumed that T-domain took part in the formation of the pores or promoted the formation of them by the MRT. These planar bilayer data are in accordance with the calcein leakage data on liposomes.

AFM revealed two different types of defects in the supported lipid bilayers: (*i*) big holes, partially edged with "heights", and (*ii*) small depressions or holes surrounded by circular "ramparts". As was shown with the use of biospecific AFM, these "heights" and "ramparts" are the MRT molecules either embedded into the bilayer or, possibly, adsorbed by it.

Summing up all the obtained data, one may assume that the process of formation of defects in lipid bilayers by the MRTs at acidic pH's could include the following stages. First, the MRTs adsorb on the surface of the bilayer. Then they insert into the bilayer, oligomerize in it, thus making penetration of low-molecular weight substances possible. We have shown that HMP used as a carrier module in the MRTs can cause oligomerization of the MRTs because the oligomeric circular structures can be observed in the supported lipid bilayers after incubation with a complete MRT containing the DT T-domain (Fig. 4B) and with a truncated MRT lacking the DT T-domain (Fig. 4C), whereas the both MRTs contained the HMP module. Subsequent processes, presumably fusion of these channels and subsequent expansion of the pores, lead to formation of big holes which diameters, up to 50–200 nm, are sufficient for escape of macromolecules. Oligomerization can be caused also by the DT T-domain: it was shown that DT forms oligomers in membranes with a variable stoichiometry creating pores with sizes depending on its concentration [40]. If a milieu located behind the opposite side of the bilayer has higher pH, so diffusion would begin to increase pH in the acidic compartment, so a part of MRT molecules which remained free, non-inserted, would be able to restore its previous conformation which was at neutral pH and escape from the acidic compartment, whereas the another part of the MRT molecules would remain inserted into the bilayer[1].

Acknowledgements

This work was supported by grants from the Dutch-Russian (NWO-RFFI) Scientific Cooperation Program (grant # 047.017.025), U.S. Civilian Research and Development Foundation (grant # RUB-02-2663-MO-05), and Russian Foundation for Basic Research (grant # 06-04-49273 and 06-04-48523).

References

[1] U. Testa, R. Riccioni, M. Biffoni, D. Diverio, F. Lo-Coco, R. Foa, C. Peschle, A.E. Frankel, Diphtheria toxin fused to variant human interleukin-3 induces cytotoxicity of blasts from patients with acute myeloid leukemia according to the level of interleukin-3 receptor expression, Blood 106 (7) (2005) 2527–2529.

[2] D.A. Vallera, D.A. Todhunter, D.W. Kuroki, Y. Shu, A. Sicheneder, H. Chen, A bispecific recombinant immunotoxin, DT2219, targeting human CD19 and CD22 receptors in a mouse xenograft model of B-cell leukemia/lymphoma, Clin. Cancer Res. 11 (10) (2005) 3879–3888.

[3] D.A. Todhunter, W.A. Hall, E. Rustamzadeh, Y. Shu, S.O. Doumbia, D.A. Vallera, A bispecific immunotoxin (DTAT13) targeting human IL-13 receptor (IL-13R) and urokinase-type plasminogen activator receptor (uPAR) in a mouse xenograft model, Protein Eng. Des. Sel. 17 (2) (2004) 157–164.

[1] The fact that DT T-domain containing chimeras remain inserted into lipid membranes after pH adjustment to neutral values was demonstrated by Nizard et al [41].

[4] M. Ichinose, X.H. Liu, N. Hagihara, R.J. Youle, Extracellular Bad fused to toxin transport domains induces apoptosis, Cancer Res. 62 (5) (2002) 1433–1438.
[5] A.A. Rosenkranz, V.G. Lunin, P.V. Gulak, O.V. Sergienko, M.A. Shumiantseva, O.L. Voronina, D.G. Gilyazova, A.P. John, A.A. Kofner, A.F. Mironov, D.A. Jans, A.S. Sobolev, Recombinant modular transporters for cell-specific nuclear delivery of locally acting drugs enhance photosensitizer activity, FASEB J. 17 (9) (2003) 1121–1123.
[6] D.G. Gilyazova, A.A. Rosenkranz, P.V. Gulak, V.G. Lunin, O.V. Sergienko, Y.V. Khramtsov, K.N. Timofeyev, M.A. Grin, A.F. Mironov, A.B. Rubin, G.P. Georgiev, A.S. Sobolev, Targeting cancer cells by novel engineered modular transporters, Cancer Res. 66 (21) (2006) 10534–10540.
[7] F.M. Foss, P. Bacha, K.E. Osann, M.F. Demierre, T. Bell, T. Kuzel, Biological correlates of acute hypersensitivity events with DAB(389)IL-2 (denileukin diftitox, ONTAK) in cutaneous T-cell lymphoma: decreased frequency and severity with steroid premedication, Clin. Lymphoma 1 (4) (2001) 298–302.
[8] A.E. Frankel, D.R. Fleming, P.D. Hall, B.L. Powell, J.H. Black, C. Leftwich, R. Gartenhaus, A phase II study of DT fusion protein denileukin diftitox in patients with fludarabine-refractory chronic lymphocytic leukemia, Clin. Cancer Res. 9 (10) (2003) 3555–3561.
[9] N.H. Dang, F.B. Hagemeister, B. Pro, P. McLaughlin, J.E. Romaguera, D. Jones, B. Samuels, F. Samaniego, A. Younes, M. Wang, A. Goy, M.A. Rodriguez, P.L. Walker, Y. Arredondo, A.T. Tong, L. Fayad, Phase II study of denileukin diftitox for relapsed/refractory B-cell non-Hodgkin's lymphoma, J. Clin. Oncol. 22 (20) (2004) 4095–4102.
[10] A.E. Frankel, B.L. Powell, P.D. Hall, L.D. Case, R.J. Kreitman, Phase I trial of a novel diphtheria toxin/granulocyte macrophage colony-stimulating factor fusion protein (DT388GMCSF) for refractory or relapsed acute myeloid leukemia, Clin. Cancer Res. 8 (5) (2002) 1004–1013.
[11] F.M. Foss, M.N. Saleh, J.G. Krueger, J.C. Nichols, J.R. Murphy, Diphtheria toxin fusion proteins, Curr. Top. Microbiol. Immunol. 234 (1998) 63–81.
[12] R.J. Kreitman, Immunotoxins for targeted cancer therapy, AAPS J. 8 (3) (2006) E532–E551.
[13] B.L. Kagan, A. Finkelstein, M. Colombini, Diphtheria toxin fragment forms large pores in phospholipid bilayer membranes, Proc. Natl. Acad. Sci. U. S. A. 78 (8) (1981) 4950–4954.
[14] J.J. Donovan, M.I. Simon, R.K. Draper, M. Montal, Diphtheria toxin forms transmembrane channels in planar lipid bilayers, Proc. Natl. Acad. Sci. U. S. A. 78 (1) (1981) 172–176.
[15] A. Wiedlocha, I.H. Madshus, H. Mach, C.R. Middaugh, S. Olsnes, Tight folding of acidic fibroblast growth factor prevents its translocation to the cytosol with diphtheria toxin as vector, EMBO J. 11 (13) (1992) 4835–4842.
[16] P.O. Falnes, S. Choe, I.H. Madshus, B.A. Wilson, S. Olsnes, Inhibition of membrane translocation of diphtheria toxin A-fragment by internal disulfide bridges, J. Biol. Chem. 269 (11) (1994) 8402–8407.
[17] K.J. Oh, L. Senzel, R.J. Collier, A. Finkelstein, Translocation of the catalytic domain of diphtheria toxin across planar phospholipid bilayers by its own T domain, Proc. Natl. Acad. Sci. U. S. A. 96 (15) (1999) 8467–8470.
[18] J. Ren, K. Kachel, H. Kim, S.E. Malenbaum, R.J. Collier, E. London, Interaction of diphtheria toxin T domain with molten globule-like proteins and its implications for translocation, Science 284 (5416) (1999) 955–957.
[19] R. Ratts, H. Zeng, E.A. Berg, C. Blue, M.E. McComb, C.E. Costello, J.C. vanderSpek, J.R. Murphy, The cytosolic entry of diphtheria toxin catalytic domain requires a host cell cytosolic translocation factor complex, J. Cell Biol. 160 (7) (2003) 1139–1150.
[20] K. Sandvig, B. van Deurs, Delivery into cells: lessons learned from plant and bacterial toxins, Gene Ther. 12 (11) (2005) 865–872.
[21] F. Szoka Jr., D. Papahadjopoulos, Procedure for preparation of liposomes with large internal aqueous space and high capture by reverse-phase evaporation, Proc. Natl. Acad. Sci. U. S. A. 75 (9) (1978) 4194–4198.
[22] A.A. Rosenkranz, Y.N. Antonenko, O.A. Smirnova, G.K. Yurov, B.S. Naroditsky, A.S. Sobolev, Avian adenovirus induces ion channels in model bilayer lipid membranes, Biochem. Biophys. Res. Commun. 236 (3) (1997) 750–753.
[23] T. Puntheeranurak, C. Stroh, R. Zhu, C. Angsuthanasombat, P. Hinterdorfer, Structure and distribution of the *Bacillus thuringiensis* Cry4Ba toxin in lipid membranes, Ultramicroscopy 105 (1–4) (2005) 115–124.
[24] A.A. Sobko, E.A. Kotova, Y.N. Antonenko, S.D. Zakharov, W.A. Cramer, Effect of lipids with different spontaneous curvature on the channel activity of colicin E1: evidence in favor of a toroidal pore, FEBS Lett. 576 (1–2) (2004) 205–210.
[25] M. Tortonese, M. Kirk, Characterization of application specific probes for SPMs, Proc. SPIE 3009 (1997) 53–60.
[26] S. Roes, F. Mumm, U. Seydel, T. Gutsmann, Localization of the lipopolysaccharide-binding protein in phospholipid membranes by atomic force microscopy, J. Biol. Chem. 281 (5) (2006) 2757–2763.
[27] X.E. Cai, J. Yang, Molecular forces for the binding and condensation of DNA molecules, Biophys. J. 82 (1) (2002) 357–365.
[28] P. Mueller, D.O. Rudin, H.T. Tien, W.C. Wescott, Reconstitution of cell membrane structure in vitro and its transformation into an excitable system, Nature 194 (1962) 979–980.
[29] S. Nir, J.L. Nieva, Interactions of peptides with liposomes: pore formation and fusion, Prog. Lipid Res. 39 (2) (2000) 181–206.
[30] B.P. Ceresa, S.L. Schmid, Regulation of signal transduction by endocytosis, Curr. Opin. Cell Biol. 12 (2) (2000) 204–210.
[31] S. Lin, Y.M. Wang, L.S. Huang, C.W. Lin, S.M. Hsu, C.K. Lee, Dynamic response of glucagon/anti-glucagon pairs to pulling velocity and pH studied by atomic force microscopy, Biosens. Bioelectron. 22 (6) (2007) 1013–1019.
[32] H. Gao, X.X. Zhang, W.B. Chang, Study on the interaction in single antigen–antibody molecules by AFM, Front Biosci. 10 (2005) 1539–1545.
[33] P. Hinterdorfer, W. Baumgartner, H.J. Gruber, K. Schilcher, H. Schindler, Detection and localization of individual antibody–antigen recognition events by atomic force microscopy, Proc. Natl. Acad. Sci. U. S. A. 93 (8) (1996) 3477–3481.
[34] A. Raab, W. Han, D. Badt, S.J. Smith-Gill, S.M. Lindsay, H. Schindler, P. Hinterdorfer, Antibody recognition imaging by force microscopy, Nat. Biotechnol. 17 (9) (1999) 901–905.
[35] M.E. Browning-Kelley, K. Wadu-Mesthrige, V. Hari, G.Y. Liu, Atomic force microscopy study of specific antigen/antibody binding, Langmuir 13 (1997) 343–350.
[36] O. Ouerghi, A. Touhami, A. Othmane, H. Ben Ouada, C. Martelet, C. Fretigny, N. Jaffrezic-Renault, Investigating antibody–antigen binding with atomic force microscopy, Sensor Actuator, B Chem. 84 (2002) 167–175.
[37] A. Bonamore, A. Farina, M. Gattoni, M.E. Schinina, A. Bellelli, A. Boffi, Interaction with membrane lipids and heme ligand binding properties of Escherichia coli flavohemoglobin, Biochemistry 42 (19) (2003) 5792–5801.
[38] A.C. Rinaldi, A. Bonamore, A. Macone, A. Boffi, A. Bozzi, A. Di Giulio, Interaction of *Vitreoscilla* hemoglobin with membrane lipids, Biochemistry 45 (13) (2006) 4069–4076.
[39] C.C. Cruickshank, R.F. Minchin, A.C. Le Dain, B. Martinac, Estimation of the pore size of the large-conductance mechanosensitive ion channel of *Escherichia coli*, Biophys. J. 73 (4) (1997) 1925–1931.
[40] J.C. Sharpe, E. London, Diphtheria toxin forms pores of different sizes depending on its concentration in membranes: probable relationship to oligomerization, J. Membr. Biol. 171 (3) (1999) 209–221.
[41] P. Nizard, A. Chenal, B. Beaumelle, A. Fourcade, D. Gillet, Prolonged display or rapid internalization of the IgG-binding protein ZZ anchored to the surface of cells using the diphtheria toxin T domain, Protein Eng. 14 (6) (2001) 439–446.